Xu, X., Wisnom, M., Sun, X., Rev, T., & Hallett, S. (2018). Experimental determination of Through-Thickness Compression (TTC) enhancement factor for Mode II fracture energy. *Composites Science and Technology*, *165*, 66-73. https://doi.org/10.1016/j.compscitech.2018.06.012

The manuscript has been accepted for publication in Composites Science and Technology

Experimental Determination of Through-Thickness Compression (TTC) Enhancement Factor for Mode II Fracture Energy

Xiaodong Xu*, Michael R. Wisnom, Xiaoyang Sun, Tamas Rev, Stephen R. Hallett

Bristol Composites Institute (ACCIS), University of Bristol, University Walk, Bristol BS8 1TR, United Kingdom

Abstract

Mode II fracture energy, G_{IIC}, is a critical parameter for determining the propagation of delamination in composite laminates. Its value can be affected by Through-Thickness Compression (TTC) stress acting on the crack tip and here this effect has been studied using IM7/8552 carbon/epoxy laminates with cut central plies. External TTC loads were applied through bi-axial testing. Unidirectional (UD) cut-ply specimens were used to determine the TTC enhancement factor, η_G, for G_{IIC}. A similar enhancement effect was also found in Quasi-isotropic (QI) specimens with 2 extra cut central 0° plies inserted into the layup. The TTC enhancement factor was implemented in a Finite Element Analysis (FEA) framework using cohesive interface elements, showing that the determined η_G can be successfully used to model the effect of TTC on delamination.

Keywords: B. Delamination; B. Fracture toughness; C. Finite element analysis (FEA); Bi-axial testing.

* Corresponding author. Tel.: +44 (0)117 33 15796.
E-mail address: xiaodong.xu@bristol.ac.uk (X. Xu)

1 Introduction

Laminated composite materials have outstanding in-plane properties, but typically low interlaminar properties. This characteristic is due to the fact that fibres lying in the plane of a laminate do not provide reinforcement through the thickness, so the laminate relies on the relatively weak resin to carry loads in between its laminae. Delamination is a major cause of failure in composite laminates, which can cause separation without breaking the fibres. Accurate prediction of delamination initiation and propagation is of considerable importance since it is a critical failure mode for many composite structures. Delamination can occur due to many causes [1], such as through-thickness tensile loading, geometry and discontinuities e.g. at free edges and ply drops.

Composite structures for load carrying applications are often subjected to multi-axial loading conditions, with a significant volume of work having been done on delamination under Through-Thickness Compression (TTC) stresses [2-10]. This is particularly relevant to the design of bolted joints [11] and components prone to impact. Fracture mechanics approaches are usually adopted to predict delamination, based on strain energy release rate analysis. Wisnom et al. [2] demonstrated that for glass/epoxy specimens with cut central plies, Mode II fracture energy is apparently not constant, but increases with specimen thickness, which can be explained through the presence of TTC stresses, according to the current study. Cui et al. [3] described the increase of G_{IIC} due to TTC enhancement, ΔG_{IIC}, empirically:

$$\Delta G_{\mathrm{IIC}} = -\eta_{\mathrm{G}} \sigma_{33} G_{\mathrm{IIC}} \tag{1}$$

where η_{G} is the TTC enhancement factor for G_{IIC}, σ_{33} is the TTC stress.

It is difficult to apply and maintain the TTC loads in the standardised Mode II fracture testing configuration, e.g. the End Notched Flexure (ENF) tests following the

ASTM D7905 [12]. Therefore, only a few papers are available on the TTC enhancement factor for Mode II fracture energy G_{IIC}. In the existing literature, there are three ways to apply TTC loads. The first method is through the introduction of hydrostatic pressure. Rhee [4] applied hydrostatic pressure to CU125NS non-woven graphite/epoxy filament wound Unidirectional (UD) thick-walled cylindrical pressure vessels. A compliance method was used to calculate the fracture energy, which increased by 35% when the applied hydrostatic pressure was increased from 0.1 MPa to 200 MPa. Cartié et al. [5] conducted 4-point ENF tests under hydrostatic pressure. They demonstrated that G_{IIC} of IM7/977-2 carbon/epoxy laminates increased linearly by up to 25% when hydrostatic pressure increased to 90 MPa. It is extremely hard to apply hydrostatic pressures in a test configuration, hence special test facilities are needed. The main limitation of this method is that the hydrostatic pressure locally creates a complex tri-axial stress state, making it difficult to determine the exact TTC stress applied to the delamination interface. Once the crack is open, the previously applied TTC pressure will be cancelled out by the same hydrostatic pressure acting on the new crack surface in the opposite direction. The second method is through the design of specimen geometry. An early attempt was to use E-glass/913 glass/epoxy and XAS/913 carbon/epoxy central cut-ply and tapered specimens under in-plane tensile loads [3]. Internal TTC stresses are created due to the discontinuity within the specimen, which can enhance G_{IIC}. Another effort was made to apply transverse compressive loads to edge-cracked off-axis specimens to generate local transverse stresses at the crack tip [6]. The transverse compressive stresses were normal to the in-plane matrix crack, and they are equivalent to the internal TTC stresses applied normal to the delamination interface in the cut-ply tests [3], assuming transverse isotropy. G_{IIC} was enhanced up to fourfold for the S2/8552

glass/epoxy laminates [6]. The common issue with these methods is that the TTC stress distribution [3] or the transverse stress distribution [6] is not uniform due to the geometrical discontinuity. The directly applied external TTC load component also increases with the applied resultant load in Ref. [6]. The average local TTC stress [3] or transverse compressive force [6] needs to be determined by a Finite Element Analysis (FEA). The third method is through mechanical clamping, such as the modified transverse crack tensile IM7/8552 specimens tested with a bolted clamping assembly in Ref. [10]. A disadvantage with such mechanical clamping is that the external TTC loads are difficult to measure accurately, the applied TTC stresses have to be determined empirically and the applied TTC stresses cannot be maintained constant throughout the test due to Poisson's effect. In an alternative method to applying the TTC stress, Gan et al. [7] developed a simple bi-axial test in which the external TTC loads can be accurately measured and maintained throughout the tests. They used this to determine the TTC enhancement factor η_f for interlaminar shear strength for IM7/8552 carbon/epoxy laminates, but the TTC enhancement factor or G_{IIC} was not studied.

UD laminates with cut central plies across the full width can be used to study delamination propagation [2, 3]. The existing literature [2-6, 10] reported to study the TTC enhancement effect on G_{IIC} for delamination propagation are all based on UD laminates. Results for specimens with stacking sequences other than UD are lacking.

In this paper, the TTC enhancement effect on G_{IIC} has been studied by means of bi-axial testing. The TTC enhancement factor for G_{IIC} is determined with UD IM7/8552 carbon/epoxy laminates with cut central plies. A set of Quasi-isotropic (QI) specimens with 2 extra cut central 0° plies across the full width were also tested to investigate the TTC enhancement effect for the same 0°/0° interface within a different layup.

The current study extends the previous work on the TTC enhancement factor on interlaminar shear strength [7] to cover the TTC enhancement factor on G_{IIC}. The characterisation of the two TTC enhancement factors is crucial for the accurate prediction of delamination initiation and propagation. Compared with the existing methods [3-6, 10], the current bi-axial test method can maintain constant applied TTC loads throughout the tests. All experimental results fall on the same linear regression line, confirming a consistent and significant TTC enhancement effect on Mode II fracture energy. The determined TTC enhancement factor is implemented in an FEA framework using cohesive interface elements and is able to simulate successfully the experimentally observed behaviour.

2 Experimental configuration

The material used in the current study is Hexcel's Hexply® IM7/8552 carbon/epoxy UD pre-preg, with a nominal ply thickness of 0.125 mm. Two panels with different stacking sequences were made. One was a 40-ply UD $[0]_{40}$ plate, with 8 central plies cut across the full width. The other plate had a layup of $[(45/90/-45/0)_4(0)]_s$ - a QI stacking sequence with 2 extra 0° plies at the mid-plane that were cut across the full width. The central 0° pre-preg plies were cut with a sharp blade and laid up with no gaps, such that only a minimum amount of resin could flow into the cut during curing. Panels were cured according to the manufacturer's specification. The measured thicknesses of the two panels after cure were close to the nominal specimen thicknesses. Both panels were then cut into 10 mm wide strips using a diamond coated wheel cutter. All specimens were 300 mm in length, with a 100 mm gauge length and 100 mm on both ends bonded with glass/epoxy end tabs.

For the uni-axial tensile testing without external TTC loads, an Instron 250 kN

hydraulic-driven test machine was used. The specimen was placed vertically, with the top actuator fixed, while the bottom actuator moved under displacement control, at a rate of 1 mm/min. For the tensile testing with external TTC loads, the same bi-axial testing rig as in Ref. [7] was used, which is equipped with four independent hydraulic-driven Zwick/Roell 100 kN actuators mounted horizontally on a flat T-slotted steel base, as shown in Figure 1 a). The current tests were bi-axial, because both loads and displacements were applied and monitored independently via two pairs of actuators, namely, actuators (y_1, y_2) in the axial loading direction and (x_1, x_2) in the orthogonal through-thickness loading direction. Because the longitudinal actuators (y_1, y_2) could not be brought very close together due to the presence of the transverse actuators, customised fixtures and jaws were used, the same as those used previously [7], made from EN24 high tensile steel. The two jaws are each connected by two steel extension arms via two M20 bolts. Six M8 high tensile bolts are used for tightening each jaw. The extension arms were clamped by the hydraulic grips on the longitudinal actuators (y_1, y_2) which were under displacement control, at a rate of 1 mm/min in each direction.

The previous fixtures were adapted to the current tests by introducing a new pair of indenters gripped in the two transverse actuators (x_1, x_2). External TTC loads were applied via the newly designed indenters, as shown in Figure 1 a), to generate a relatively uniform external stress field over their length of 25 mm. There is no radius at the corners of the indenter in the length direction. The heat treated steel indenters have flat profiles in contact with the specimen surfaces, hence the compression region has a dimension of 25 mm by 10 mm. The applied external TTC stress is defined as the average value over the compression area of 250 mm^2, which is fairly uniform according to the Finite Element (FE) results in Section 5. After the specimen was clamped in the

desired position longitudinally, the two transverse indenters (x_1, x_2) were brought in until they lightly touched the specimen surfaces. One indenter was held at a fixed position during the test, while the other indenter was put under load control, as shown in Figure 1 b). Any potential bending due to this asymmetric compression arrangement in the through-thickness direction was minimised by having the two M20 bolts which loosely connect the jaws to the extension arms and allow for some movement in the transverse direction [7]. Constant external TTC loads were maintained throughout the tests to compensate for any specimen deformation due to Poisson's effect. The steel indenters' contacting surfaces were well polished, and no friction between the indenters and the specimen surfaces was considered. This is because the applied TTC loads relevant to the determination of TTC enhancement factor are moderate, ranging from 5 to 15 kN. If a coefficient of friction $\mu = 0.15$ [13] is taken for the current symmetrically loaded UD laminates, the total friction force applied to the half specimen is small compared to the measured failure load at delamination propagation (within 3%).

3 Experimental results

3.1 Uni-axial tensile tests

A total of 4 QI specimens with 2 extra cut central 0° plies and 8 UD specimens with 8 central cut-plies were tested without externally applied TTC loads. A typical load vs. cross-head displacement curve without TTC is shown in Figure 2 a). The response is slightly non-linear at the beginning, because the displacements were measured at the cross heads. Sometimes a very small load drop can be seen, and this is believed to be caused by non-critical damage, such as the resin breaking at the cut. Then a large load drop occurs, which was observed to be delamination propagation. In most cases, delamination propagates simultaneously at the both interfaces above and below the cut

plies. Sometimes delaminations do not propagate simultaneously from both sides of the cut, and another load drop can be observed right after the first large load drop. The load at the first large load drop is taken to calculate the net-section delamination propagation stress. The final load drop represents fibre breakage, marking the end of the test.

A closed form solution can be derived to work out the fracture energy, G_C, for the QI laminates with 2 extra cut central 0° plies, assuming simultaneous delaminations above and below the cut plies. Considering uniform in-plane tensile response yields Equation 2 based on the method introduced in Ref. [2].

$$G_C = \frac{\sigma_{net}^2 (h-t)}{4E^*} - \frac{\sigma_{net}^2 (h-t)^2}{4E_{lam} h} \tag{2}$$

where h is the total specimen thickness, t is the thickness of the cut plies, σ_{net} is the average net-section stress at the first large load drop from the measured specimen width and the thickness of continuous plies, E_{lam} = 67.5 GPa is the longitudinal Young's modulus before delamination and E^* = 61.6 GPa is the longitudinal Young's modulus of the remaining load carrying plies in the totally delaminated laminate.

For UD central cut-ply laminates , Equation 2 can be reduced to a special closed form solution as shown in Equation 3 [3] with E_{11} = 161 GPa.

$$G_C = \frac{\sigma_{net}^2 (h-t) t}{4E_{11} h} \tag{3}$$

There are two sources of TTC stresses generated in the current tests, which are the internal and external TTC stresses. From the FE results without external TTC loading in Ref. [3], it is known that the delamination at the central 0° cut plies is pure Mode II because there is a small internal TTC stress component at the cut. Therefore, the critical strain energy release rate evaluated from Equations 1 and 2 are equal to $G_{IIC\_n}^{int}$, which is the enhanced Mode II fracture energy with no externally applied TTC. Table 1 shows

the results from the uni-axial tensile tests (at 0 kN TTC loads). Because the UD central cut-ply specimen and the QI specimen with 2 extra cut central 0° plies are made of the same material with the same 0°/0° delamination interface, $G_{\mathrm{IIC_n}}^{\mathrm{int}}$values derived from the both tests are similar. The measured values are higher than the reported value G_{IIC} = 0.8 N/mm from ENF testing [14], due to the enhancement effect from local internal TTC stresses at the cut [3].

3.2 Bi-axial tests

Two sets of central cut-ply specimens were tested on the bi-axial machine. The QI specimens with 2 extra cut central 0° plies were subjected to 2.5 kN, 5 kN and 10 kN applied TTC loads respectively, and the corresponding magnitude of externally applied TTC stresses are 10 MPa, 20 MPa and 40 MPa. The UD central cut-ply specimens were subjected to 5 kN, 10 kN, 15 kN and 20 kN applied TTC loads respectively, and the corresponding magnitude of externally applied TTC stresses are 20 MPa, 40 MPa, 60 MPa and 80 MPa. Three samples were tested for each case.

The typical load vs. cross-head displacement curve with TTC in Figure 2 b) appears more non-linear than those from the uni-axial tensile tests. This can be attributed to the displacements being measured at the cross heads and some slippage at the steel jaws. Typical failed QI specimens with 2 extra cut central 0° plies are shown in Figure 3. In most cases, under moderate external TTC loads, a large load drop was observed before the ultimate failure, corresponding to simultaneous delamination propagation from above and below the cut plies. Sometimes, a second load drop could be observed right after the first load drop, when delamination propagation did not happen simultaneously at both sides of the cut. The corresponding load at the first large load drop was taken to determine $G_{\mathrm{IIC\_n}}$ which is the enhanced Mode II fracture energy

with externally applied TTC. The ultimate failure is represented by a final load drop caused by either fibre failure outside the compressed region after delamination propagation, or slippage at the steel jaws at high in-plane loads after delamination propagation. In cases under high external TTC loads, there was only one load drop due to fibre fracture within the compressed region. These particular results could therefore not be used for the determination of G_{IIC_n}. The bi-axial test results of the QI specimens with 2 extra cut central 0° plies as illustrated in Table 1 exhibit a significant TTC enhancement effect on G_{IIC}. However, only a small range of external TTC loads can be applied before the failure mode switches from delamination to fibre failure, and the results are no longer relevant to the determination of the TTC enhancement factor for G_{IIC}. In contrast, the UD central cut-ply specimens can sustain a larger range of applied TTC loads, which is ideal for the determination of the TTC enhancement factor. Also shown in Table 1 is that the net-section stresses at fibre failure with TTC loads higher than 2.5 kN are slightly lower than the net-section stress at delamination propagation at 2.5 kN TTC load. This may be attributed to the fact that the delaminations at 2.5 kN TTC load blunt the in-plane stress concentrations at the cut.

4 Experimental determination of η_G

Internal TTC exists due to load transfer around the discontinuities at the cut within the specimen [3]. The axial tension loading causes material deformation due to Poisson's effect, hence an internal TTC stress is formed near the cut where the axial tension is reduced due to the discontinuity. As the specimen configuration was kept constant, it is reasonable to assume the internal TTC stress distribution remains approximately the same. This will be justified through FEA in Section 5.

The other source of TTC is applied externally through the pair of indenters during

bi-axial testing. The externally applied TTC stresses σ_{33}^{ext} can significantly enhance G_{IIC}. Figure 4 illustrates a linear regression line that fits the UD central cut-ply test results with a coefficient of determination R^2 = 0.99. Although the measured $G_{\text{IIC\_n}}$ is still affected by the internal geometric TTC stresses due to in-plane tension, the slope of the linear regression line is unaffected, assuming the internal TTC stress distribution due to the discontinuity remains the same at all applied external compressive loads. Therefore η_{G} = 0.064 MPa^{-1} can be derived from the measured $G_{\text{IIC\_ n}}$ values and $G_{\text{IIC\_n}}^{\text{int}}$= 1.08 N/mm in Table 1 according to Equation 4.

$$G_{\text{IIC\_n}} = G_{\text{IIC\_n}}^{\text{int}}(1 - \eta_{\text{G}}\sigma_{33}^{\text{ext}}) \quad (4)$$

Figure 4 also shows that the QI cut-ply test results in Table 1 follow the same linear regression line. The TTC enhancement effect is the same as that in the UD central cut-ply tests, which is as expected since the 0°/0° interfaces and materials are the same.

5 Numerical implementation of η_{G}

A Finite Element Analysis has been carried out to verify the measured TTC enhancement effect on G_{IIC} in the UD central cut-ply tests, using the explicit code LS-Dyna with cohesive interface elements. One eighth of the specimen and a quarter indenter head were modelled as shown in Figure 5. 8-node constant-stress continuum element were used. There is one element through each ply thickness (0.125 mm). The minimum mesh size in the in-plane loading direction is 0.128 mm at the cut, for both continuum and cohesive interface elements. The thickness of the cohesive interface elements is 0.01 mm. Only 6 elements were used across the model width (5 mm), because free edge effects are not relevant for these UD specimens.

Nodes at the three symmetry planes are fixed in the direction normal to the plane to apply the symmetry boundary conditions. In the length direction, the nodes at the end

of the continuous plies near the indenter head are fixed, but those at the same end of the discontinuous plies are not constrained, in order to represent a cut across the width at the specimen centre. At the beginning of the simulation, the TTC force was ramped up to reach a constant value, applied evenly over the modelled indenter head which has elastic properties (Young's modulus E = 210 GPa and Poisson's ratio v = 0.3). Automatic surface to surface contact was used between the indenter head and the specimen surface to transfer the external TTC loads. No friction was considered in the FEA because the effect of friction is small in the current bi-axial tests and can be neglected. After the target TTC force was reached, uniform displacements were applied horizontally to the nodes at the end away from the indenter at a constant rate of 1 mm/s.

In the FEA, cohesive interface elements were used to simulate delaminations. A mixed-mode traction-separation law was applied in a user-defined material subroutine for cohesive interface elements [8, 15]. There are two failure criteria as shown in Equation 5. One is a stress-based criterion for damage initiation. When the through-thickness stress is compressive, its enhancement effect on damage initiation is reflected by updating the interlaminar shear strength [8]. The other criterion is an energy-based criterion for full debonding.

$$\begin{cases} \left(\dfrac{\max(\sigma_{33},0)}{S_{\text{normal}}}\right)^2 + \left(\dfrac{\sqrt{\sigma_{13}^2+\sigma_{23}^2}}{S_{\text{shear}}}\right)^2 = 1 & \text{for damage initiation} \\ \dfrac{G_{\text{I}}}{G_{\text{IC}}} + \dfrac{G_{\text{II}}}{G_{\text{IIC}}} = 1 & \text{for fully debonding} \end{cases} \tag{5}$$

where σ_{33} is the FE simulated TTC stress, σ_{13} and σ_{23} are the shear stress components, S_{normal} is the through-thickness tensile strength, S_{shear} is the interlaminar shear strength, G_{I} is Mode I elastic strain energy release rate, G_{IC} is Mode I fracture energy, G_{II} is Mode II elastic strain energy release rate and G_{IIC} is Mode II fracture energy.

The Mode II failure criterion has also been updated according to Equation 6 as the failure propagation criteria for cohesive interface elements under TTC stresses [8].

$$\begin{cases} S_{\text{shear}_\text{n}} = S_{\text{shear}} - \eta_f \sigma_{33} \\ G_{\text{IIC\_n}} = G_{\text{IIC}}(1 - \eta_\text{G} \sigma_{33}) \end{cases} \quad (6)$$

where η_f is the TTC enhancement factor for interlaminar shear strength S_{shear}. For the current IM7/8552 carbon/epoxy material, η_f = 0.3 has been previously determined [7]. The value of the TTC enhancement factor for G_{IIC} of η_G = 0.064 MPa^{-1} has been determined in the current paper. G_{IIC} = 0.8 N/mm [14]. $S_{\text{shear}_\text{n}}$ and $G_{\text{IIC\_n}}$ are the TTC enhanced values. Figure 6 [8] shows the traction-separation relationship under TTC stresses with independent TTC enhancement effects on S_{shear} and G_{IIC}.

The properties of the cohesive interface elements and continuum elements used are shown in Table 2. The input G_{IIC} value in Table 2 is different from the measured value $G_{\text{IIC\_n}}^{\text{int}}$ in Table 1, because the measured value reflects the enhancement effect from the internal TTC stresses. A penalty stiffness value of K = 100,000 N/mm^3 is used for the cohesive elements. The mass is scaled up in all FE models by a factor of about 100, 000 to reduce the run time. Dynamic effects have been checked to be sufficiently low so as not to affect the results. The model timestep is 9×10^{-7} s.

In Figure 7, the TTC stress distributions along a line of nodes near the cut/continuous plies interface up to the edge of the indenter head are compared between the FE models without any external TTC loading and with a 5 kN applied TTC load. Firstly, the TTC stress distribution caused by the externally applied 5 kN TTC load without any in-plane loading is fairly uniform near the cut (dashed line in black). Only close to the edge of the indenter does the TTC stress slightly increase. The TTC stress is close to the average TTC stress of 20 MPa calculated using the nominal compressed area and the externally applied 5 kN TTC load. Secondly, a resultant TTC stress

distribution (long dashed line in green) can be generated by superimposing the internal TTC stress distribution before delamination (dotted line in blue) from the model without any externally applied TTC loading and the TTC stress distribution (dashed line in black) from the model only under the externally applied 5 kN TTC load without any in-plane loading. The superimposed TTC stress distribution is similar to the numerically generated TTC stress distribution before delamination (solid line in red) from the model under the externally applied 5 kN TTC load with in-plane loading. This justifies the previous assumption that the internal TTC stress distribution caused by the geometrical discontinuity remains approximately the same for the same specimen configuration with and without applied external TTC loads. Thirdly, the internal TTC stress distribution before delamination from the model without any applied external TTC loading indicates that tension is present at the very tip of the cut. However, this only happens at the end nodes due to the geometrical discontinuity, and immediately turns to compression at the adjacent nodes. The contribution of the end nodes is small and can be neglected.

The FE predicted load drop for delamination propagation is close to the measured first load drop. The predicted load vs. displacement response is stiffer than measured, because cross-head displacements were used in the experiments, and there was some slippage at the steel jaws. The modelling results under different applied TTC stresses are also compared against the experimental results in Figure 8. The FE results agree with the experimental results well. To be consistent with the experiments, the FE generated G_{IIC_n} values are also back calculated according to Equation 3. The applied TTC stresses σ_{33}^{ext} are calculated from the externally applied TTC loads and the nominal compressed area in the FEA. The load at which delamination propagates significantly was used to determine the TTC enhanced Mode II fracture energy G_{IIC_n} in the FEA.

This also corresponds to a load drop on the numerical load vs. displacement curve. The experimental displacements were measured at the cross heads, so the apparent experimental stiffness is less than the numerical stiffness. Fibre failure after delamination propagation is not considered in the FEA, so no effort was made to predict the final experimental load drop. The modelling results are not sensitive to the mesh size. For instance, for the model without externally applied TTC loads, a further refined mesh with a minimum mesh size of 0.064 mm yields the same G_{IIC_n}.

The FE results demonstrate that the experimentally measured TTC enhancement factor η_G can be used in the existing FEA framework [8], and can potentially be used in the analysis of delamination in composite structures under TTC.

6 Discussion

In the FEA, the input TTC enhancement law for G_{IIC} is linear as shown in Equation 5, but the FE generated G_{IIC_n} vs. σ_{33}^{ext} curve is not strictly a straight line as shown in Figure 8. This may be because the first delamination in the models does not lead to unstable delamination propagation immediately. Since significant delamination propagation was taken to determine G_{IIC_n}, the short delay could cause the slight nonlinearity. However, the FE generated G_{IIC_n} vs. σ_{33}^{ext} curve is close to a straight line, as observed experimentally.

In the original formulation of the TTC enhanced cohesive interface element [8], three possible TTC enhancement laws were investigated including the independent enhancement of interlaminar shear strength and fracture energy in Equation 5 as used here. Here a test has now been developed that has accurately determined the TTC enhancement factor for interlaminar Mode II fracture energy for the IM7/8552 carbon/epoxy laminates to be η_G = 0.064 MPa^{-1}. This is close to the previously

measured equivalent value of 0.079 MPa^{-1} for intra-laminar Mode II fracture energy for the S2/8552 glass/epoxy laminates [6]. The currently measured η_G = 0.064 MPa^{-1} is also of the same order of magnitude as the suggested value of η_G = 0.025 MPa^{-1} for the T300/914 carbon/epoxy laminates from a previous numerical study [8]. These values are however quite different to η_G = 0.0035 MPa^{-1} for IM7/8552 carbon/epoxy laminates in Ref. [10], which used a bolted clamping assembly. The current bi-axial testing method uses directly applied TTC loads which can be ensured to be maintained constant throughout the test up to failure, without any influence from Poisson's effect.

The enhancement factor for interlaminar shear strength in the TTC enhancement law in Equation 5 was previously measured to be η_f = 0.3 in Ref. [7]. There is thus clear evidence of independence of the interlaminar shear strength and fracture energy enhancement due to TTC and for the commonly used IM7/8552 material system, these enhancement factors have now been accurately characterised for future use. There are various possible explanations for the TTC enhancement mechanisms. The enhancement effect on interlaminar shear strength has been attributed to being analogous to an internal frictional effect [7, 8]. The enhancement effect on G_{IIC} was also found to be caused by the change of the damage process zone under TTC stresses [10]. Interlaminar friction after de-cohesion may further influence the TTC enhancement effects [9]. There is scope to investigate these enhancement mechanisms in the future, but the current paper mainly focuses on the experimental determination of the enhancement factor η_G.

To generate a good range of externally applied TTC stresses for the determination of the TTC enhancement factor η_G for G_{IIC}, one should design the indenters carefully depending on the available bi-axial machine and the specimen configuration used. If the indenter is too long, the high TTC load may introduce significant friction. If the indenter

is too short, the applied TTC stress may be less uniform. Narrow indenters could also trigger earlier fibre failure, limiting the range of usable TTC loads.

7 Conclusions

A bi-axial test method has been developed for the determination of the Through-Thickness Compression (TTC) enhancement factor η_G for Mode II fracture energy G_{IIC}, using UD central cut-ply specimens. For the IM7/8552 carbon/epoxy laminates, the TTC enhancement factor for G_{IIC} is $\eta_G = 0.064$ MPa^{-1}. The same η_G has been determined from independent tests on IM7/8552 QI specimens with 2 extra cut central 0° plies, since the 0°/0° delamination interfaces and the materials are the same.

The determined η_G has been successfully implemented in the existing FEA framework using cohesive interface elements, and has been shown to simulate closely the UD central cut-ply test results. This implies that the modelling approach can be applied in the analysis of delamination in composite structures under TTC.

References

[1] M.R. Wisnom, The role of delamination in failure of fibre-reinforced composites, Philosophical Transactions of the Royal Society A: Mathematical, Physical and Engineering Sciences 370 (2012) 1850-1870.

[2] M.R. Wisnom, On the increase in fracture energy with thickness in delamination of unidirectional glass fibre-epoxy with cut central plies, Journal of Reinforced Plastics and Composites 11(8) (1992) 897-909.

[3] W. Cui, M.R. Wisnom, M.I. Jones, Effect of through thickness tensile and compressive stresses on delamination propagation fracture energy, Journal of Composites, Technology and Research 16(4) (1994) 329-335.

[4] K.Y. Rhee, Hydrostatic pressure effect on the fracture toughness of unidirectional (0-deg) graphite/epoxy laminated composites, J. Compos Mater. 34(7) (2000) 599-613.

[5] D. Cartié, P. Davies, M. Peleau, I.K. Partridge, The influence of hydrostatic pressure on the interlaminar fracture toughness of carbon/epoxy composites, Composites Part B: Engineering 37(4) (2006) 292-300.

[6] Q. Bing, C.T. Sun, Effect of compressive transverse normal stress on mode II fracture toughness in polymeric composites, International Journal of Fracture 145(2) (2007) 89-97.

[7] K.W. Gan, S.R. Hallett, M.R. Wisnom, Measurement and modelling of interlaminar shear strength enhancement under moderate through-thickness compression, Composites Part A: Applied Science and Manufacturing 49 (2013) 18-25.

[8] X. Li, S.R. Hallett, M.R. Wisnom, Predicting the effect of through-thickness compressive stress on delamination using interface elements, Composites Part A: Applied Science and Manufacturing 39(2) (2008) 218-230.

[9] Z. Zou, H. Lee, A cohesive zone model taking account of the effect of through-thickness compression, Composites Part A: Applied Science and Manufacturing 98 (2017) 90-98.

[10] G. Catalanotti, C. Furtado, T. Scalici, G. Pitarresi, F.P. van der Meer, P.P. Camanho, The effect of through-thickness compressive stress on mode II interlaminar fracture toughness, Composite Structures 182(Supplement C) (2017) 153-163.

[11] J.H. Stockdale, F.L. Matthews, The effect of clamping pressure on bolt bearing loads in glass fibre-reinforced plastics, Composites 7(1) (1976) 34-38.

[12] ASTM, Standard, D7905/D7905M-14, Standard test method for determination of the mode II interlaminar fracture toughness of unidirectional fiber-reinforced polymer matrix composites, ASTM International, West Conshohocken, PA, USA, 2014.

[13] S. Matsunaga, T. Matsubara, W.-X. Wang, Y. Takao, Effects of reciprocation number on the friction behaviors of carbon/epoxy for various fiber orientations and high contact pressures, 13th International Conference on Composite Materials, Beijing, China, 2001.

[14] T.K. O'Brien, W.M. Johnston, G.J. Toland, Mode II interlaminar fracture toughness and fatigue characterization of a graphite epoxy composite material, NASA/TM–2010-216838, 2010.

[15] W.-G. Jiang, S.R. Hallett, B.G. Green, M.R. Wisnom, A concise interface constitutive law for analysis of delamination and splitting in composite materials and its application to scaled notched tensile specimens, International Journal for Numerical Methods in Engineering 69(9) (2007) 1982-1995.

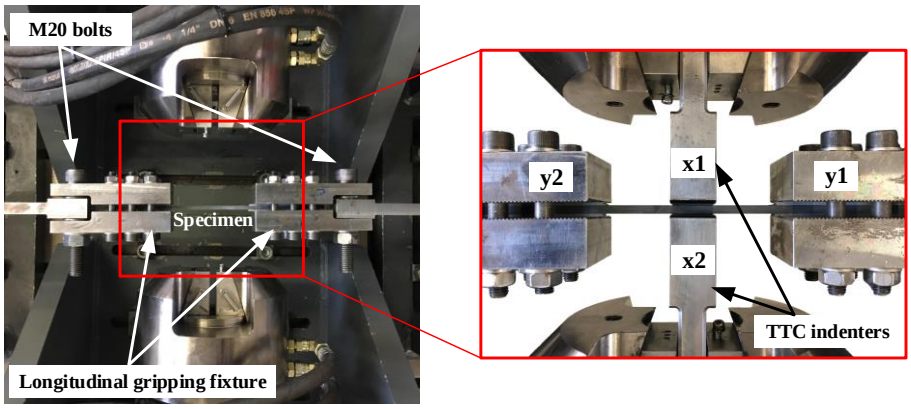

a) Bi-axial test fixtures.

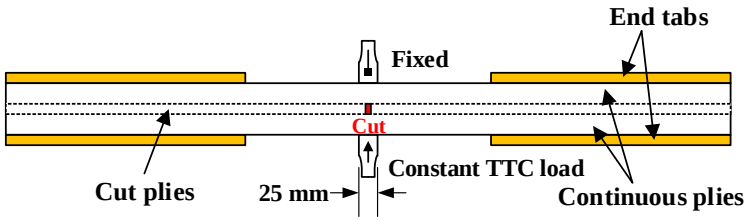

b) Schematic of the specimen with TTC indenters (not to scale).

Figure 1. Bi-axial test set-up.

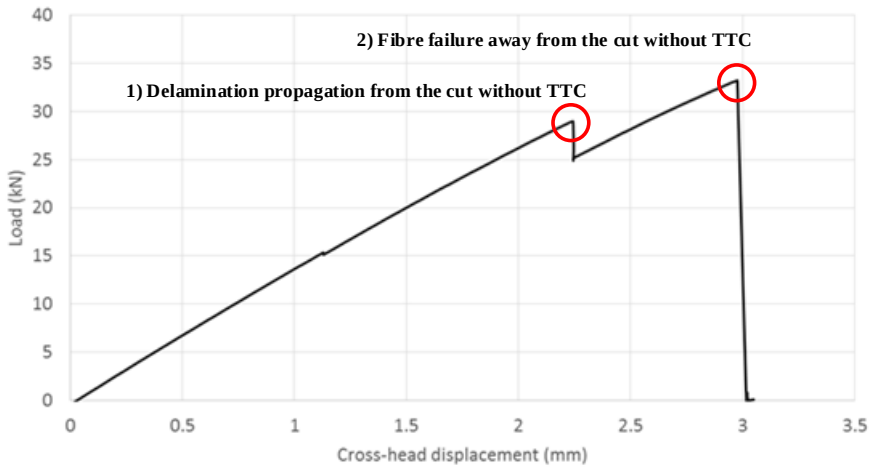

a) A typical load vs. cross-head displacement curve from a QI central cut-ply test without externally applied TTC.

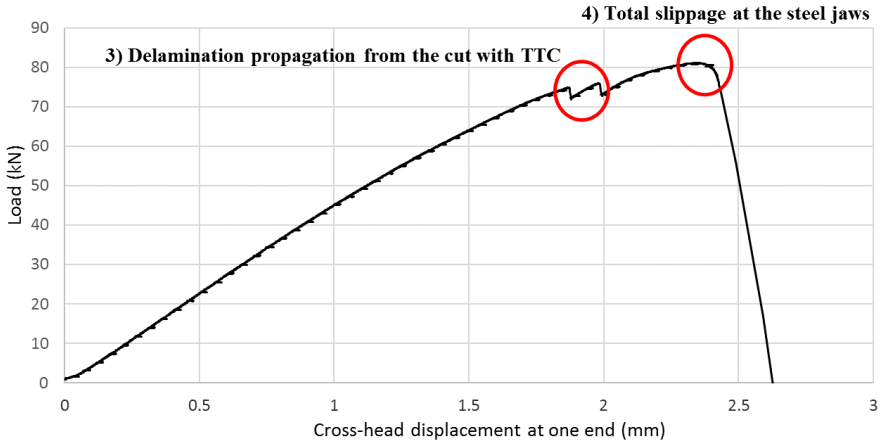

b) The measured load vs. cross-head displacement response in a UD central cut-ply test with externally applied 10 kN TTC.

Figure 2. Typical load vs. cross-head displacement response in central cut-ply tests.

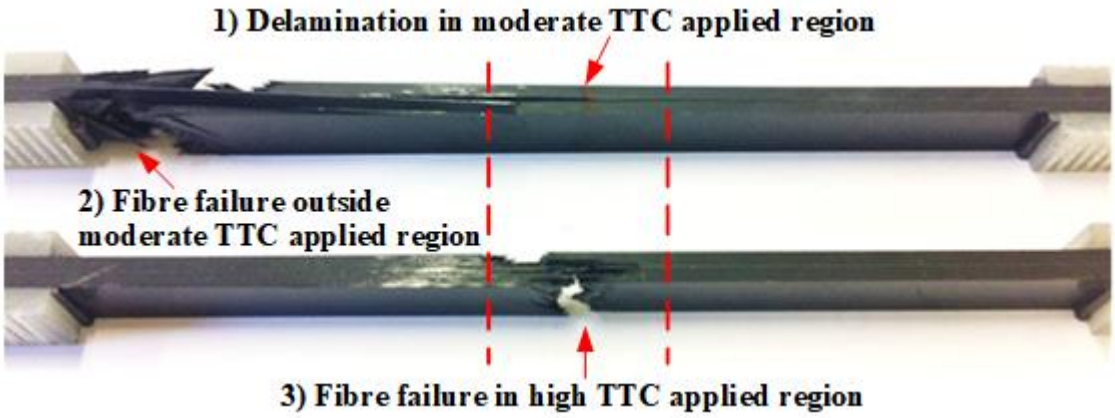

Figure 3. Typical failed QI central cut-ply specimens with externally applied TTC.

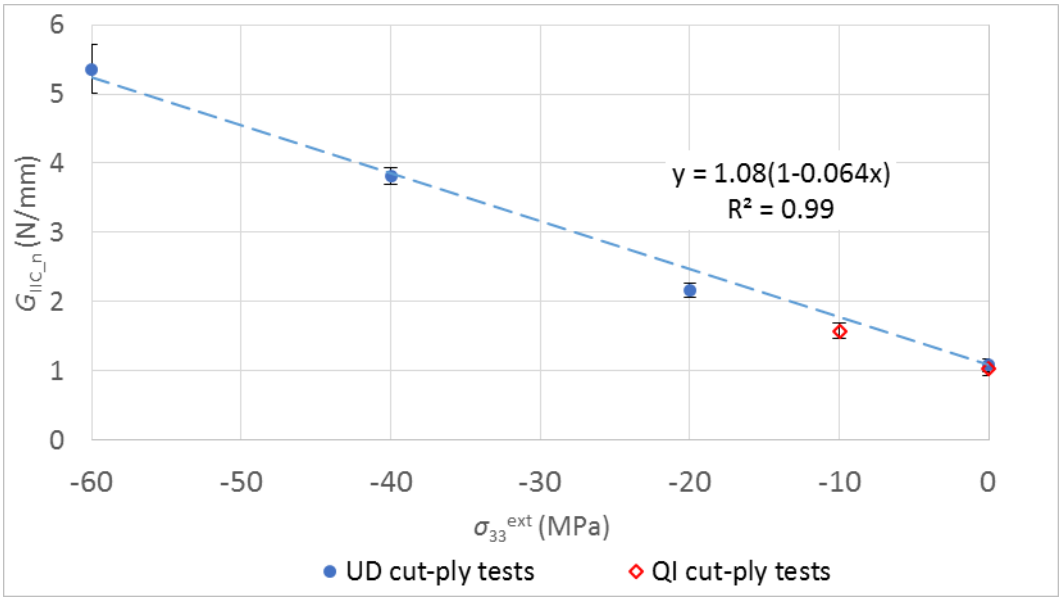

Figure 4. TTC enhancement effect on G_{IIC} in UD and QI central cut-ply tests.

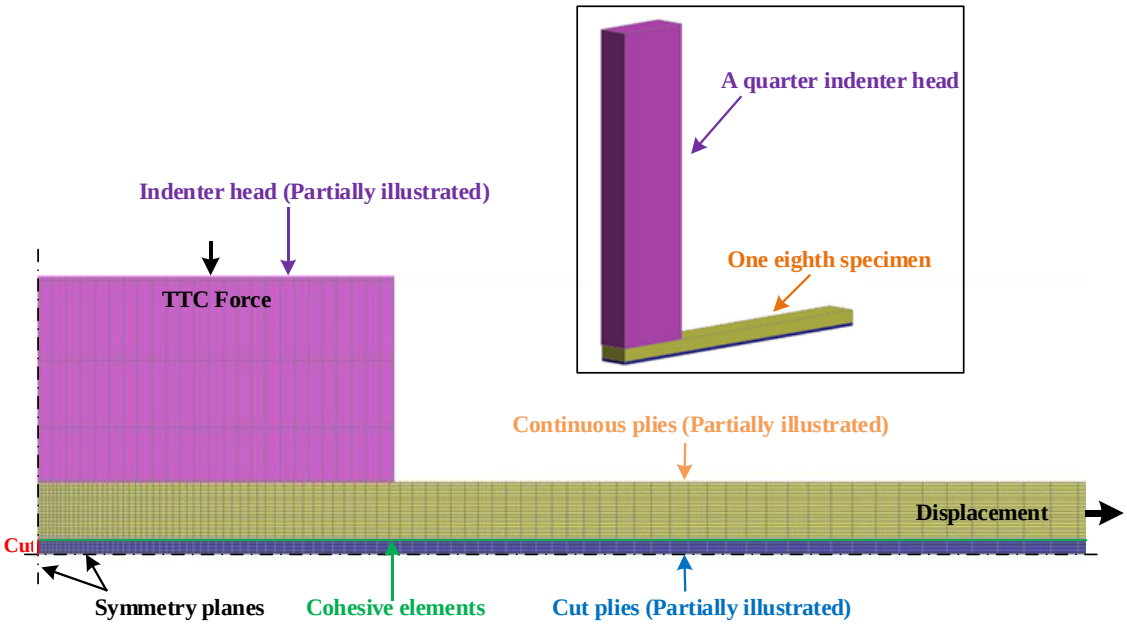

Figure 5. A typical UD central cut-ply FE model.

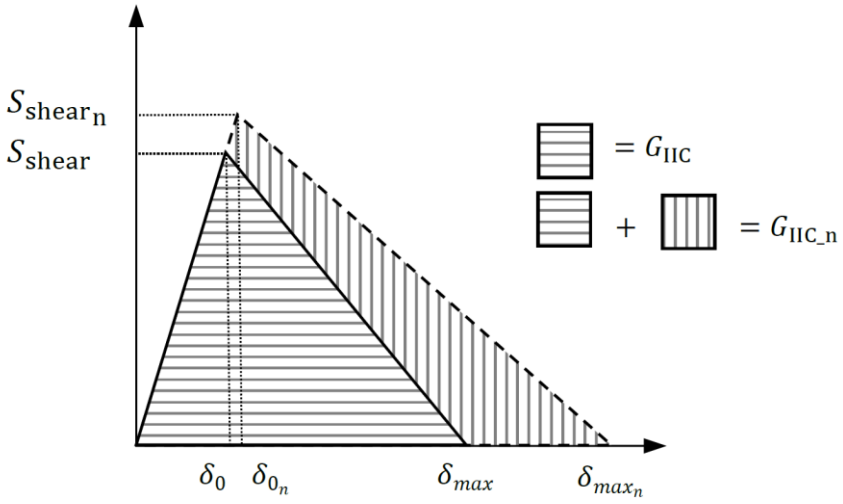

Figure 6. Mode II traction-separation law under TTC stresses for cohesive interface elements, where δ_0 and δ_{max} are the shear deformation at delamination initiation and failure respectively, δ_{0_n} and δ_{max_n}, are the enhanced values under TTC stresses [8].

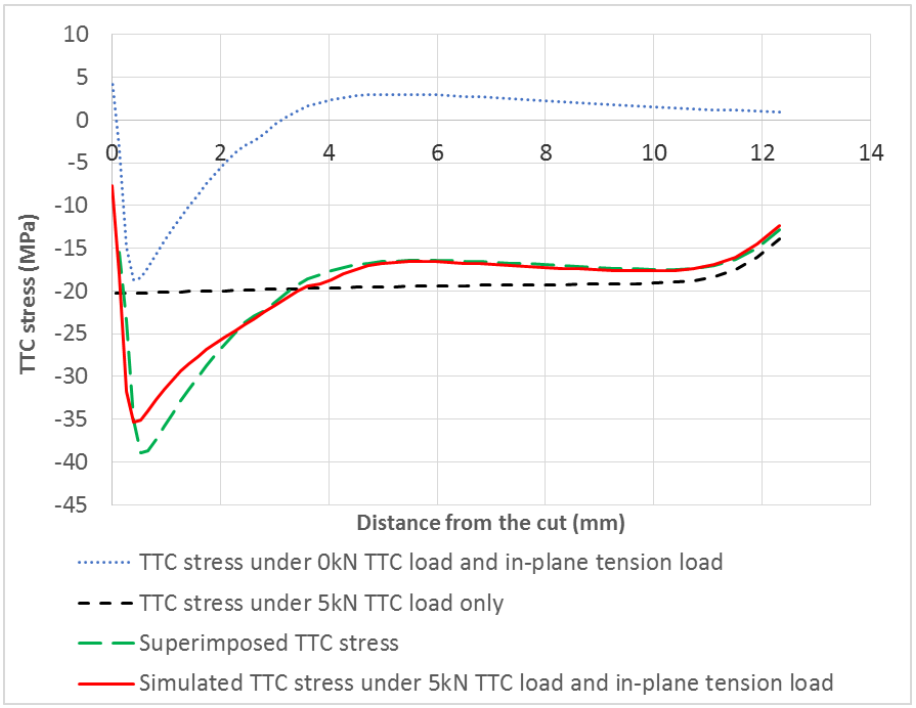

Figure 7. TTC stress distributions in the UD central cut-ply FE models.

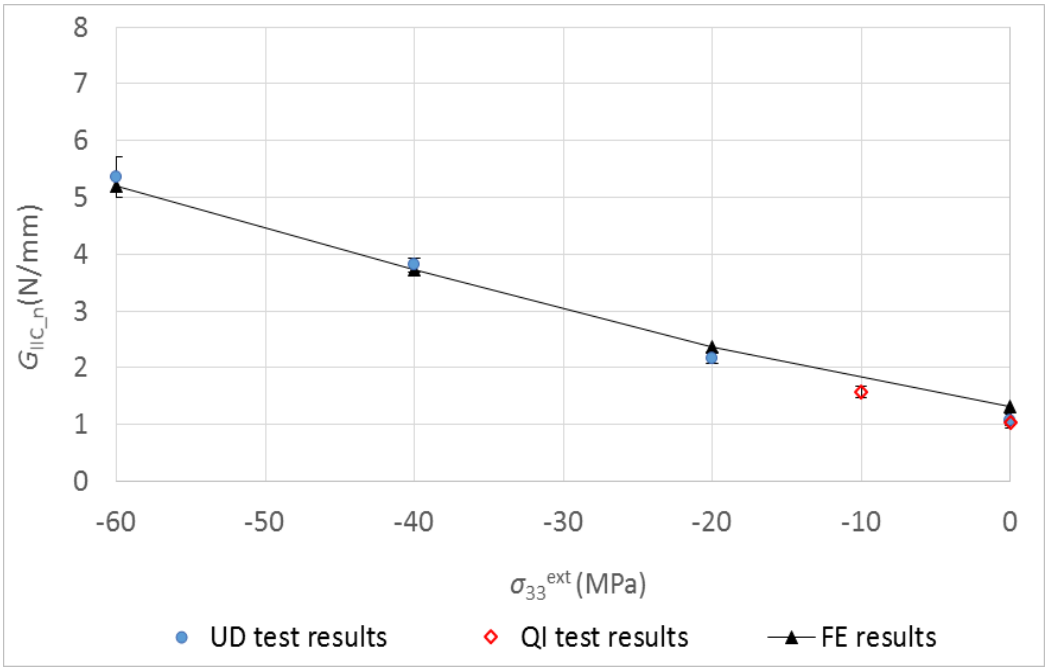

Figure 8. Simulated TTC enhancement effect on G_{IIC} correlates to the experiments.

Table 1. Summary of experimental results.

Layup	TTC load [kN]	$\lvert\sigma_{33}^{\mathrm{ext}}\rvert$[MPa]	σ_{net} (C.V.) [MPa]	$G_{\mathrm{IIC\_n}}$(C.V.) [N/mm]
UD	0	0	932 (4.6%)	1.08 (9.1%)*
	5	20	1318 (2.3%)	2.17 (4.5%)
	10	40	1743 (1.6%)	3.81 (3.2%)
	15	60	2071 (6.3%)	5.36 (11.9%)
	20	80	2069 (10.9%)	Fibre failure
QI	0	0	674 (4.5%)	1.03 (9.0%)*
	2.5	10	834 (3.3%)	1.58 (6.7%)
	5	20	793 (3.7%)	Fibre failure
	10	40	801 (0.3%)	Fibre failure

* $G_{\mathrm{IIC\_n}}^{\mathrm{int}}$ values from the uni-axial tensile tests without externally applied TTC loads

Table 2. The properties of cohesive interface and continuum elements.

Properties of cohesive interface elements					
G_{IC} [N/mm]	G_{IIC} [N/mm]	S_{normal} [MPa]	S_{shear} [MPa]	η_f	η_{G} [MPa^{-1}]
0.2	0.8 [14]	60	90	0.3 [7]	0.064
Properties of continuum elements					
E_{11} [GPa]	E_{22}=E_{33} [GPa]	G_{12}=G_{13} [GPa]	G_{23} [GPa]	υ_{12}=υ_{13}	υ_{23}
161	11.4	5.17	3.98	0.320	0.436